Atomic imaging of thin films with surface x-ray diffraction: introducing DCAF

2008 J. Phys.: Condens. Matter 20 445006

(http://iopscience.iop.org/0953-8984/20/44/445006)

J. Phys.: Condens. Matter **20** (2008) 445006 (7pp) doi:10.1088/0953-8984/20/44/445006

Atomic imaging of thin films with surface x-ray diffraction: introducing DCAF

M Björck, C M Schlepütz, S A Pauli, D Martoccia, R Herger and P R Willmott

Swiss Light Source, Paul Scherrer Institut, CH-5232 Villigen PSI, Switzerland

Received 20 August 2008
Published 10 October 2008
Online at stacks.iop.org/JPhysCM/20/445006

Abstract

A direct method for the retrieval of electron density maps from surface x-ray diffraction data is presented and its performance is evaluated. The method, DCAF (difference map using the constraints of atomicity and film shift), is based on the difference map iteration scheme and uses, apart from the traditional constraints of atomicity, positivity and film thickness, a novel constraint, which we have named the 'film shift', whereby the real space solution is shifted up by an out-of-plane unit cell size of the underlying bulk substrate material if the topmost region of the same thickness contains insignificant electron density. This relaxes the film thickness constraint, which is necessarily loose in order to accommodate structural uncertainties at the film–substrate interface due to intermixing, roughness, and heteroepitaxial strain.

DCAF's performance was evaluated by retrieval of the electron density distribution from a real data set, recorded from a five-monolayer film of $LaAlO_3$ on $SrTiO_3$, which resulted in an electron density in good agreement with the previously solved structure. Importantly, the stability and reproducibility of the final solution compares favorably with constraint combinations in which the film shift projection is omitted, highlighting the power of this new method. In addition, an example of a full structural solution for a three-monolayer-thick film of $La_{1-x}Sr_xMnO_3$ on $SrTiO_3$ is presented, where DCAF electron density retrieval followed by model building and refinement was conducted.

It will be shown that DCAF can be successfully applied to thin films for retrieving physically meaningful electron densities, and that it can also serve as a starting point for subsequent structure refinement.

1. Introduction

Surface x-ray diffraction (SXRD) is uniquely capable of providing the precise atomic arrangement at surfaces of single crystals and at thin film interfaces [1]. Structural information is of especially high importance in modern condensed matter physics, such as in strongly correlated materials, where subtle movements of atoms can have a fundamental effect on the material's physical properties. For increasingly complex systems, ordinary model fitting approaches become more difficult, if not essentially impossible, due to the large number of free parameters to be refined.

An ideal way to analyze an x-ray diffraction pattern would be to take its inverse Fourier transform to yield the three-dimensional electron density. This is not possible because of the phase problem, which is due to the fact that the measured intensities only contain information about the magnitude of the scattered wave and not the phase. However, the information loss caused by the missing phase can be compensated by iterative optimization methods which force the electron density to agree with the measured data as well as *a priori* information. These methods are called phase retrieval methods or direct methods. In bulk crystallography, the *a priori* information included in these methods are usually that the electron density should be positive and atomic-like [2].

In contrast to bulk x-ray diffraction, SXRD aims at determining the structure of a single crystalline surface or film, which is periodic in the two in-plane directions and aperiodic in the out-of-plane direction. This aperiodicity gives rise to continuous streaks of intensity in the out-of-plane direction, called diffraction rods. Since the diffraction rods are continuous, they can be sampled more finely than the lowest sampling frequency necessary to get a real space volume with the same extension as that for the assumed out-of-plane size of the unknown surface structure, which is equivalent to the Nyquist frequency. This makes it possible to get a real space

volume larger than the unknown surface structure in the out-of-plane dimension. Consequently, there exists a region in real space where the inverted electron density can be assumed to be zero. This procedure is called oversampling and is an indispensable part of optical phase retrieval methods [3]. The region where the unknown part of the electron density is considered to be non-zero is denoted as the support.

The first articles on direct methods for SXRD were published by Marks an co-workers [4–7] at the end of the 1990s. Their method is quite elaborate, using a combination of phase retrieval techniques and a genetic algorithm to explore multiple solutions. Later work by Saldin and co-workers [8–10] showed that it is possible to use a rather simple and transparent phase retrieval scheme, namely the error-reduction algorithm suggested by Fienup [11, 12], combined with the knowledge that the electron density is a positive quantity which differs from the bulk in a small region close the surface. This method, called PARADIGM, has solved the surface structure of Au(110)-(2 × 1) [13] and two reconstructions in the Sb/Au(110) system [14, 15]. The starting point of the above mentioned methods consists of a random initialization of the phases or the electron density, rendering it possible to check for the existence of multiple solutions. At about the same time as Saldin and co-workers formulated PARADIGM, Yacoby and co-workers developed the coherent Bragg rod analysis (COBRA) [16–18]. This method also uses positivity and knowledge about the film thickness. However, it differs in the Fourier space projections, as it uses the assumption that the phase of the unknown part, the thin film, should vary more slowly than the phase of the bulk contribution. Also, in contrast to Marks's and Saldin's methods, COBRA is initialized with a starting model for the unknown structure.

Recently, there have been significant advances in the understanding and performance of direct methods [3, 19–26]. These new techniques have some common features that make them very effective. The first is the use of hybrid input–output [12] or similar algorithms, e.g., the difference map [22, 23], that have a low probability to get trapped in local minima. Secondly, most of the direct methods use a dynamical support where the region that contains the object is modified in some manner during the phase retrieval process.

The aim of this work has been to develop a direct method for SXRD that can, with a random initialization of the phases of the complex structure factors, retrieve the correct phases and thereby produce consistent maps of the electron density of thin films with sub-atomic resolution. We use the difference map iteration scheme in combination with atomicity and a new type of dynamical support, named the film shift. Our method is hereafter referred to as DCAF (difference map using the constraints of atomicity and film shift). The following sections explain DCAF in detail and explore its effectiveness compared to other constraint combinations in retrieving the electron densities from real data acquired with SXRD from thin film samples.

2. Direct method formulation

2.1. Background

The signal collected in SXRD experiments contains contributions from the bulk of the sample as well as from the thin film or surface structure under investigation. The former is usually known and the structure factors F_{bulk} from the truncated bulk can be calculated. The total structure factor can then be expressed in terms of the unknown surface structure, having an electron density ρ,

$$F_{\text{tot}}(\rho) = F_{\text{surf}} + F_{\text{bulk}} = \text{FT}[\rho] + F_{\text{bulk}}, \tag{1}$$

where FT denotes the Fourier transform. The quantity ρ is non-zero only in a finite region given by the thickness of the unknown surface structure. It is this finiteness in the out-of-plane direction which allows for the oversampling of the corresponding diffraction signal which aids us to solve the structure. In the remainder of this section we will present DCAF in detail, which can be employed to retrieve the electron density, ρ.

2.2. Projections

A central concept in direct methods is that of constraints, which describe an *a priori* property of the system to be fulfilled by a solution. In x-ray diffraction, the system is described by an electron density. The set of those electron densities compatible with a given constraint forms a subset of the entire search space of possible electron densities. Mathematically, the application of a constraint can be formulated in terms of a projection operator [3], which assigns to a given point in the search space the nearest point of the corresponding constraint subset.

Direct method algorithms use a combination of these projection operators (henceforth referred to as projections) to find points of the search space which satisfy all corresponding constraints simultaneously. In other words, the intersection of all constraints forms the solution subset. Depending on the particular choice of constraints and their overlap, the solution subset may contain exactly one solution, several (multiple) solutions, or no solutions at all. It is therefore the applicability and effectiveness of the employed projections which determine the success of the direct method in solving a particular problem. In the following, the specific real space and Fourier space projections used in this work are discussed in detail.

2.2.1. Fourier space. For an electron density to be a valid solution, the most important constraint is that its Fourier transform agrees with the measured structure factor magnitudes. Due to the phase problem, the respective phases cannot be constrained and are thus left unchanged. The magnitude projection is written as

$$\mathbf{P_M}(\rho) = \text{IFT}\left[|F_{\text{meas}}| \cdot \frac{F_{\text{tot}}(\rho)}{|F_{\text{tot}}(\rho)|} - F_{\text{bulk}}\right], \tag{2}$$

where the bulk contribution has been subtracted such that only the structure factors of the unknown part remain. This step has

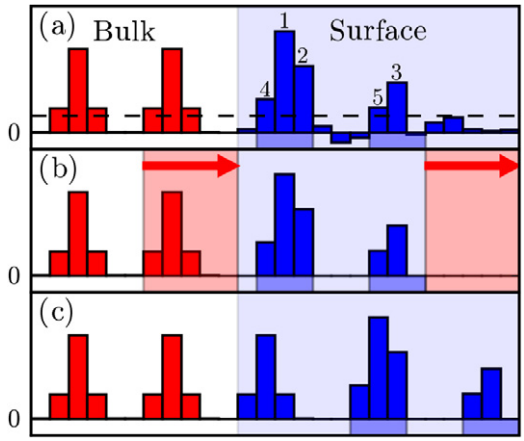

Figure 1. An illustration of the real space projection steps. (a) The starting electron density distribution. The area beneath the two atoms found is highlighted. The result of the atomicity and positivity projection is shown in (b). The electron density after the application of the film shifting projection is shown in (c).

(This figure is in colour only in the electronic version)

one important consequence, however: the value of $|F_{\text{meas}}|$ must be known on an absolute scale, given by the definition of F_{bulk}.

The magnitude projection implicitly applies a second constraint on the electron density. Since the diffraction pattern is assumed to be centrosymmetric (in SXRD, only diffraction signals above the surface can be measured), its Fourier transform results in a real-valued electron density, even though the structure factors are complex numbers.

Finally, one problem is how to treat missing data points in the diffraction pattern since the corresponding structure factors cannot be constrained directly. The approach used in this work is to leave those calculated structure factors unchanged.

2.2.2. Real space. The real space projection uses the following *a priori* information: the electron density is positive; the unknown part has a certain maximal extension in the out-of-plane direction; the unknown part is made up of atoms and the substrate structure is known. The positivity projection, $\mathbf{P_p}$, can be written as

$$\mathbf{P_p}\rho = \begin{cases} \rho, & \rho \geqslant 0 \\ 0, & \rho < 0. \end{cases} \tag{3}$$

The second and third points are included in a projection which we denote as the atomicity projection. The procedure for identifying atoms is based on that of Elser [22], the main difference here being that this work uses a threshold level for identifying atoms, whereas Elser used a fixed number of atoms. The different steps of the real space projection can be followed in figures 1(a) and (b). First, only a certain region, given by the maximal thickness of the unknown part, is used for the identification of atoms, the range denoted as 'Surface' in figure 1(a). The voxels in this 3D volume are then ranked according to their electron density. This is exemplified in figure 1(a) by the indices shown above the bars. Note that only the bars above the threshold are assigned an index. The first atom to be placed is centered around the voxel with the highest electron density, and, according to atomicity constraint, is also assigned an extent of v_a voxels (in the 1D example above, $v_a = 3$). Successively working down the ranking list, it is then checked that placing a new atom at the indexed position will not cause any overlapping with previously placed atoms. If the position is free, a new atom is placed there. The search for atoms finishes when the current value in the ranking list drops below the threshold level. In our example, the first atom is placed at the position marked with 1. The voxel marked with 2 has the second highest ranking, but is rejected because it would result in an overlap with the first atom. The next available position is marked with 3. All the remaining rankings would either cause an overlap with an existing atom or lie below the threshold, marked by the dashed line in figure 1(a). The last step of the projection sets the values in all voxels outside any atoms to zero. The result can be seen in figure 1(b) where the positivity projection has also been applied.

Due to the geometry of the sample, a thin film on top of a semi-infinite substrate, there is always an ambiguity as to where the film, the unknown, meets the substrate. Shifting the boundary between the bulk and unknown surface region by exactly one unit cell results in an identical overall structure, but changes the contents of the unknown electron density, producing two equally valid solutions. Our film shift projection forces a maximum filling of the entire unknown part. Thus, once the atomicity projection has been performed, it is checked whether the distance between the top atom and the upper boundary of the unknown region is larger than a bulk unit cell. If this is the case, the entire structure is shifted up, as shown by the arrows in figure 1(b), resulting in a maximum filling with atoms, figure 1(c).

2.3. The difference map

With these projections at hand, we now need an iterative algorithm which will perform the search for a solution. Elser and co-workers have developed a generalized hybrid input–output type algorithm which avoids getting trapped in local minima on its search for a global solution [23]. This so-called difference map algorithm can be written as [21–23]

$$\begin{aligned} \rho_{i+1} &= \rho_i + \beta\,[T_1(\rho_i) - T_2(\rho_i)] \\ T_1(\rho_i) &= \mathbf{P_R}\left[(1+\beta^{-1})\mathbf{P_F} - \beta^{-1}\right](\rho_i) \\ T_2(\rho_i) &= \mathbf{P_F}\left[(1-\beta^{-1})\mathbf{P_R} + \beta^{-1}\right](\rho_i), \end{aligned} \tag{4}$$

where β is a control parameter in the interval $(0, 1]$. Studies have indicated that the optimal value for β should be in the range $0.4 \leqslant \beta \leqslant 0.8$ [23]. Our own tests show no clear correlations between the number of iterations and β. Other studies [20] have seen similar behavior. All the experiments here have used $\beta = 1$, which simplifies the difference map to

$$\rho_{i+1} = \rho_i + 2\mathbf{P_R}\mathbf{P_F}\rho_i - \mathbf{P_R}\rho_i - \mathbf{P_F}\rho_i. \tag{5}$$

To monitor the progress of the algorithm, we use the difference map error [22], defined as

$$\epsilon_{\text{DM},i+1} = \|T_1(\rho_i) - T_2(\rho_i)\|\,. \tag{6}$$

The difference map, equation (4), needs a starting point for the electron density, ρ_0. Choosing a random starting point renders it possible to verify the uniqueness of the solution by repeating the search several times. Here, we assign random phases to the measured structure factor amplitudes.

$$\rho_0 = \mathrm{IFT}\left[|F_{\mathrm{meas}}|\, \mathrm{e}^{\mathrm{rand}(0,2\pi)\mathrm{i}}\right]. \tag{7}$$

2.4. Technical details

The atomicity projection is most efficient if the size of the atomic 'bins' is as small as possible. However, the electron cloud of an atom has a certain extension and shape given by the inverse Fourier transform of the atomic form factor, f. Additional broadening arises from thermal motion. In order to optimize the effectiveness of the atomic support, the mean shape of the atoms, given by the assumed composition of the unknown region, can be deconvoluted from the electron density. This is done by forming unitary structure factors, U [27].

$$|U| = \frac{F}{\sum_j f_j} \tag{8}$$

where the denominator is the sum over all atoms in the unknown part. In the two cases shown here, unitary structure factors improve the lowest achievable difference map error but do not affect the final solution.

Due to the finite sampling volume in Fourier space, the structure factors are truncated at a certain position. This truncation causes spectral leakage, ringing, in the electron density. To avoid this, a window function, $W(|Q|)$, is multiplied with the measured data. In this work a Gaussian window function, width σ_{w}, is used since this will lead to the same atomic shape as the Debye–Waller factor. The value of σ_{w} is optimized by having it as low (which gives broader atoms) as the chosen atomic support allows. In other words the total number of electrons within the atomic support for a hypothetical mean atom is maximized with regard to σ_{w}.

3. Application and evaluation

An experimental data set of $LaAlO_3$ (LAO) on $SrTiO_3$ (STO) data has been used to evaluate DCAF's ability to reconstruct the electron density. Data for $La_{1-x}Sr_xMnO_3$ (LSMO) grown on STO serve to illustrate a complete refinement process.

3.1. Details of measurements

Details of sample fabrication for the five-monolayer (ML) film of LAO on STO and the 3 ML film of LSMO on STO can be found in [28, 29]. Both samples were measured at the Material Science beamline, Swiss Light Source, Paul Scherrer Institut, Switzerland. The range in reciprocal space used for the subsequent analysis here was $h, k = 0, \ldots, 4$ and $0.3 \leqslant l \leqslant 4.5$ r.l.u. with a sampling interval of 0.025 r.l.u. for the LAO film, and $h, k = 0, \ldots, 3$ and $0.25 \leqslant l \leqslant 3.5$ r.l.u. with a sampling interval of 0.05 r.l.u. for the LSMO film. This implies that the vertical extent of one voxel corresponds to 1.30 Å and 1.67 Å for the LAO data and the LSMO data, respectively. The reciprocal lattice is defined by the cubic STO substrate, which has a bulk lattice parameter of $a = 3.9045$ Å ($2\pi/a = 1.6092$ Å^{-1}).

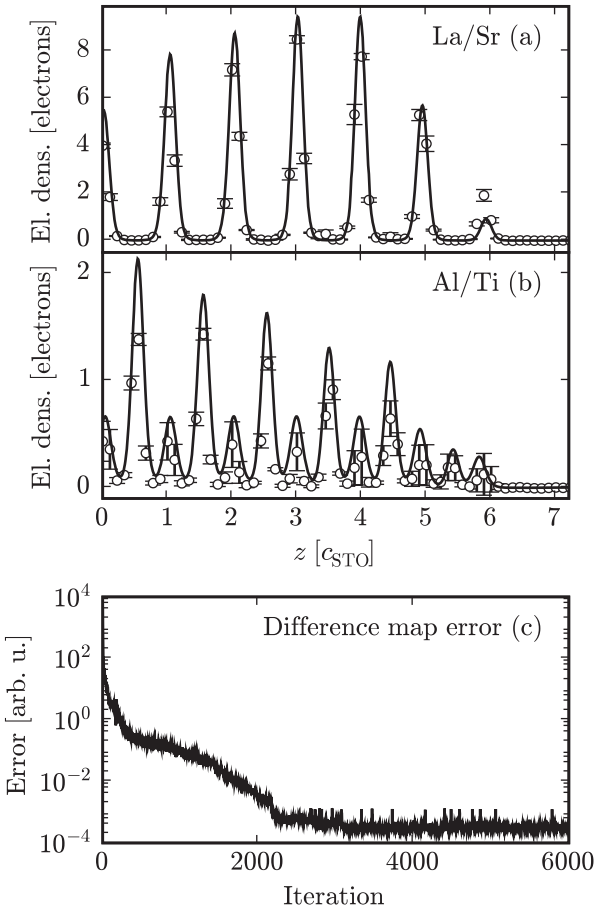

Figure 2. (a), (b) A comparison between the refined model [28] (lines) and the retrieved electron density (circles). A line scan through the electron density in the out-of-plane direction for the center of the La/Sr atoms (a) and the Mn/Ti atoms (b) is displayed. (c) The evolution of the difference map error as a function of the number of iterations.

3.2. Evaluation: LAO on STO

The data from LAO on STO was scaled using the already determined structure [28] including the corresponding scale factor. The result of a typical DCAF run is shown in figure 2. The upper two panels show the retrieved electron density (circles) as a function of out-of-plane position for two different in-plane positions corresponding to the sites for Sr/La, (a), and Ti/Al, (b). The error bars display the standard deviation of the 10 electron densities with the lowest difference map error, for a DCAF run of 6000 iterations. The parameters for DCAF are displayed in table 1. An unknown region of two STO unit cells thicker than the expected thickness of the film was chosen. The agreement between the electron density calculated from the refined parameters in [28] (full line) and the retrieved ones is good. Note that all the oxygen atoms are seen for the Ti/Al curve. The lower panel displays the difference map error, equation (6), as a function of the number of iterations. The

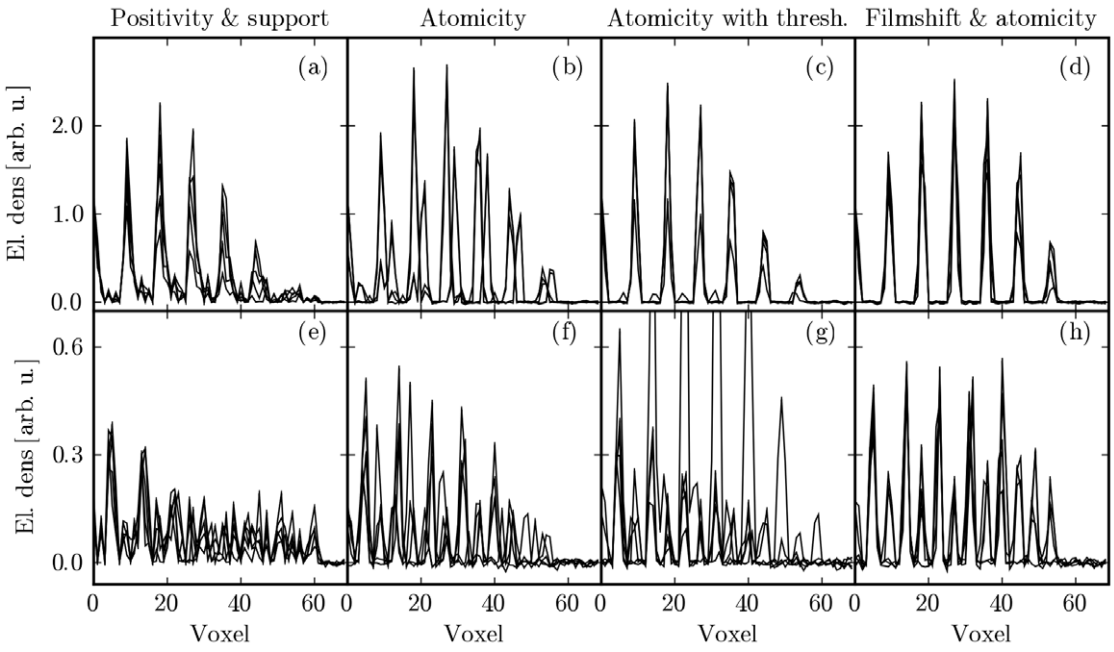

Figure 3. As-retrieved electron density distributions for the Sr/La sites (a)–(d) and the Ti/Al sites (e)–(h). Panels (a) and (e) show the use of positivity and support, (b) and (f) including atomicity with a fixed number of atoms, (c) and (g) atomicity with thresholding and (d) and (h) atomicity with thresholding and film shift. Each panel shows five different retrieval runs.

Table 1. The control parameters used by the direct method for the two different samples. The first two columns denote the thickness of the unknown region in voxels and in STO unit cells, respectively. Column 'Thresh.' gives the minimum allowed value, given as a percentage of the maximum value of the electron density, for the center value of an atom. σ_w is the width of the window function.

	Unknown region				
Sample	voxels	STO UC	Thresh. (%)	σ_w (r.l.u.)	At. size voxels
LAO	62	6.8	5	3.0	$3 \times 3 \times 3$
LSMO	36	5.1	10	2.8	$3 \times 3 \times 3$

fluctuations (above 3000 iterations) in the difference map error show that the algorithm is still searching. Thus, the problem formulation is probably slightly over-constrained, i.e., there is no intersection of the different constraint sets.

A comparison between four different constraint combinations can be seen in figure 3. The following combinations were used: positivity and a fixed thickness of the unknown region; atomicity with a fixed number of atoms; atomicity with a threshold; film shifting and atomicity with a threshold (DCAF). The first combination is similar to the direct method proposed by Saldin and co-workers [8, 9], with the exception that the difference map was used instead of the error-reduction algorithm [12]. The second implementation is an adaptation of the direct method proposed by Elser [22] to SXRD. The third combination, atomicity with a threshold (here 5% of the maximum electron density), is the first part of the real space constraint in DCAF, described in section 2.2.2. Each method was executed for 6000 iterations in five consecutive runs with random initialization.

As seen in figure 3, the quality and reproducibility of the fourth method, DCAF, is superior to the other three. The least effective combination is the first, with only positivity constraint and fixed thickness of the unknown region. More detailed tests showed that the performance of the first method can be slightly improved by choosing a very tight support. In the other three methods, the inclusion of more information, i.e. atomicity, is able to compensate for the loose support constraint. Introducing the film shift projection creates a stable solution with a more detailed structure, as seen from the resolved oxygen atoms between the Ti/Al atoms in figure 3(h).

3.3. Application: LSMO on STO

The data from LSMO did not extend as far out in reciprocal space as the LAO data. Consequently, the atomicity support was not as effective for this data set, as the size of the atomic 'bins' was larger than those for the LAO data. The intensity was normalized to an *absolute scale*, exploiting the fact that the reflectivity is equal to unity below the critical angle. The configurable parameters of DCAF are shown in table 1. Results from a typical retrieval run can be seen in figure 4, showing two electron density voxel columns, corresponding to the La/Sr and Mn/Ti positions. The oxygen atoms lie below the 10% threshold level, since the electron density peak of the oxygen atoms is shared between four voxels, and consequently they are missing in the final electron density. Multiple restarts of DCAF showed that the retrieved electron densities are reproducible with random initializations. Attempts to retrieve the electron density with lower threshold values (thereby capturing the oxygen positions) yielded unstable solutions.

The data shown in figure 4 were parametrized by adding atoms at suitable positions, while their composition and Debye–Waller factors were adjusted to give a visual agreement with the retrieved electron density. The result is seen as the

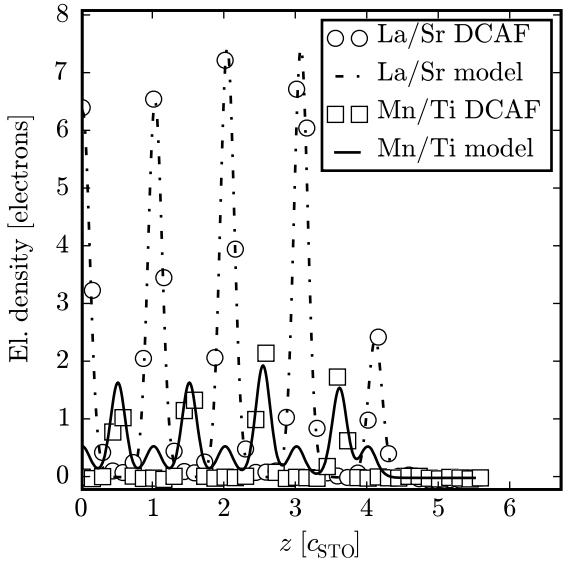

Figure 4. The retrieved electron density for the LSMO. The circles and squares show the retrieved electron density for the in-plane La/Sr positions and Mn/Ti positions, respectively, as a function of out-of-plane position. The lines show the initial model of the film obtained from this electron density.

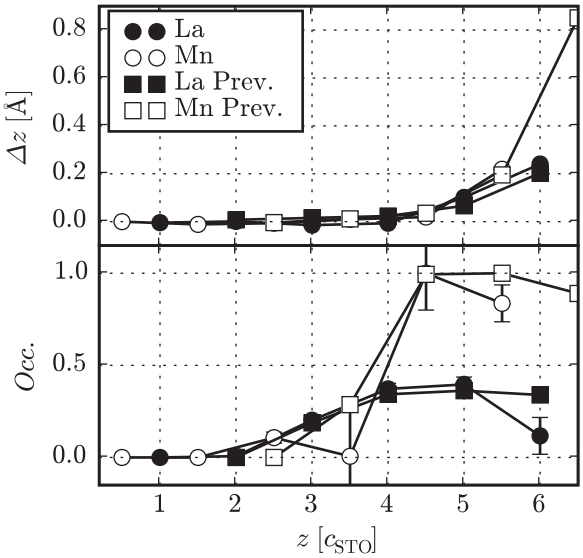

Figure 6. Comparison between the refinement presented here (circles) and previous work [29] (squares). Filled symbols denote Sr/La sites and unfilled Ti/Mn sites. The upper panel shows the displacement from the STO bulk position and the lower the site-dependent occupancy for La and Mn, respectively.

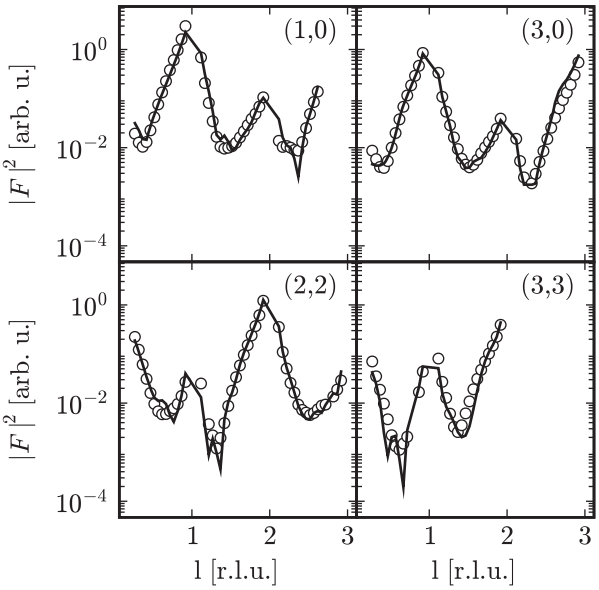

Figure 5. Four examples of the fitted diffraction rods from the LSMO film. Full lines denote the final model and the circles the measured data points.

full and dashed lines in figure 4. The oxygen atoms were included at the bulk positions, despite the fact that there were no oxygen atoms in the retrieved electron density, in order to model complete LSMO unit cells. Evaluating the *R* factor [30] for this model yielded a value of 14.6%. The final refinement was done with GenX [31], resulting in an *R* factor of 7.5%. The best fit together with the data is shown in figure 5 for four arbitrarily chosen diffraction rods. The displacement, Δz, of the atoms from the STO bulk position is shown in the upper panel of figure 6. The lower panel shows the occupancy of La and Mn. Figure 6 also includes values from a previous study by Herger and co-workers [29]. The two refinements show a good agreement except at the last layer, where the previous structural solution has an atom at the Mn sites which was not found here. The difference between the present and the previous refinement [29] is most probably due to the imposed consistency between several data sets in the latter. This is also supported with the higher *R*-factor of 8.2% found previously.

4. Conclusions

DCAF has been applied to data from two different systems: 5 ML of LAO on STO and 3 ML of LSMO on STO. The LAO was used to evaluate the performance of DCAF—the retrieved electron density was compared to independent structural refinements with good quantitative agreement. The advantage of using the film shift projection was shown in comparison with three other projection combinations, incorporating different *a priori* information. Of all the tested projection schemes, only DCAF (implementing atomicity and the film shift projection) gave the necessary detailed and reproducible results.

LSMO was used as an example of how a full structural analysis can be carried out. Starting with a direct method run to retrieve the electron density, a model of the system could be built. This starting model was subsequently refined. The final result showed good agreement with previous refinements [29].

In summary, it has been shown that DCAF can successfully retrieve accurate and reliable electron densities from thin films. In addition, the retrieved electron densities have been used as a starting point to successfully build and refine atomistic models. In the future, DCAF could very well prove to be a valuable tool for on-line analysis of SXRD data as well as providing an unbiased, objective, starting point for further, more detailed, refinements.

References

[1] Robinson I K and Tweet D J 1992 *Rep. Prog. Phys.* **55** 599
[2] Sayre D 1952 *Acta Crystallogr.* **5** 60
[3] Marchesini S 2007 *Rev. Sci. Instrum.* **78** 011301
[4] Marks L D 1999 *Phys. Rev.* B **60** 2771
[5] Marks L D, Bengu E, Collazo-Davila C, Grozea D, Landree E, Leslie C and Sinkler W 1998 *Surf. Rev. Lett.* **5** 1087
[6] Marks L D, Erdman N and Subramanian A 2001 *J. Phys.: Condens. Matter* **13** 10677
[7] Marks L D, Sinkler W and Landree E 1999 *Acta Crystallogr.* A **55** 601
[8] Saldin D K, Harder R J, Shneerson V L and Moritz W 2002 *J. Phys.: Condens. Matter* **14** 4087
[9] Saldin D K, Harder R J, Shneerson V L and Moritz W 2001 *J. Phys.: Condens. Matter* **13** 10689
[10] Saldin D K, Harder R, Volger H, Moritz W and Robinson I K 2001 *Comput. Phys. Commun.* **137** 12
[11] Fienup J R 1982 *Appl. Opt.* **21** 2758
[12] Fienup J R 1978 *Opt. Lett.* **3** 27
[13] Lyman P F, Shneerson V L, Fung R, Harder R J, Lu E D, Parihar S S and Saldin D K 2005 *Phys. Rev.* B **71** 081402
[14] Lyman P F, Shneerson V L, Fung R, Parihar S S, Johnson-Steigelman H T, Lu E D and Saldin D K 2006 *Surf. Sci.* **600** 424
[15] Fung R, Shneerson V L, Lyman P F, Parihar S S, Johnson-Steigelman H T and Saldin D K 2007 *Acta Crystallogr.* A **63** 139
[16] Sowwan Y, Yacoby Y, Pitney J, MacHarrie R, Hong M, Cross J, Walko D A, Clarke R, Pindak R and Stern E A 2002 *Phys. Rev.* B **66** 205311
[17] Yacoby Y, Pindak R, MacHarrie R, Pfeiffer L, Berman L and Clarke R 2000 *J. Phys.: Condens. Matter* **12** 3929
[18] Yacoby Y, Sowwan M, Stern E, Cross J, Brewe D, Pindak R, Pitney J, Dufrense E B and Clarke R 2003 *Physica* B **336** 39
[19] Shapiro D, Thibault P, Beetz T, Elser V, Howells M, Jacobsen C, Kirz J, Lima E, Miao H, Neiman A M and Sayre D 2005 *Proc. Natl Acad. Sci. USA* **102** 15343
[20] Thibault P, Elser V, Jacobsen C, Shapiro D and Sayre D 2006 *Acta Crystallogr.* A **62** 248
[21] Elser V 2003 *J. Phys. A: Math. Gen.* **36** 2995
[22] Elser V 2003 *Acta Crystallogr.* A **59** 201
[23] Elser V 2003 *J. Opt. Soc. Am.* A **20** 40
[24] Marchesini S, He H, Chapman H N, Hau-Riege S P, Noy A, Howells M R, Weierstall U and Spence J C H 2003 *Phys. Rev.* B **68** 140101
[25] Bunk O, Diaz A, Pfeiffer F, David C, Schmitt B, Satapathy D K and van der Veen J F 2007 *Acta Crystallogr.* **63** 306
[26] Jinsong W, Leinenweber K, Spence J C H and O'Keeffe M 2006 *Nat. Mater.* **5** 647
[27] Giacovazzo C, Monaco H L, Viterbo D, Scodari F, Gilli G, Zanotti G and Catti M 2000 *Fundamentals of Crystallography* (*IUCr Texts on Crystallography*) (Oxford: Oxford University Press)
[28] Willmott P R, Pauli S A, Herger R, Schlepütz C M, Martoccia D, Patterson B D, Delley B, Clarke R, Kumah D, Cionca C and Yacoby Y 2007 *Phys. Rev. Lett.* **99** 155502
[29] Herger R, Willmott P R, Bunk O, Schlepütz C M, Patterson B D, Kumah D, Clarke R, Yacoby Y and Döbeli M 2007 *Phys. Rev.* B **77** 085401
[30] Hamilton W C 1965 *Acta Crystallogr.* **18** 502
[31] Björck M and Andersson G 2007 *J. Appl. Cryst.* **40** 1174